PREDICTION OF SNOW FAILURE: MISSION IMPOSSIBLE?

Achille Capelli[1]*, Ingrid Reiweger[2], and Jürg Schweizer[1]

[1] *WSL Institute for Snow and Avalanche Research SLF, Davos Dorf, Switzerland*
[2] *Institute of Mountain Risk Engineering, Department of Civil Engineering and Natural Hazards, BOKU University of Natural Resources and Life Sciences, Wien, Austria*

ABSTRACT: Slab avalanches are caused by a crack forming and propagating in a weak layer within the snow cover, which eventually causes the detachment of the overlying cohesive slab. Predicting the nucleation of the initial failure is therefore needed to assess the probability of avalanche release. Failure in heterogeneous materials, such as snow, is normally preceded by a progressive damage process. Monitoring this progressive damage should allow predicting the failure point. We performed snow failure experiments in a cold laboratory and studied the damage process measuring the acoustic emissions (AE) generated by the damage (micro-cracking). Moreover, we simulated the damage process and the resulting AE with a fiber bundle model (FBM) accounting for the disorder as well as the time dependent sintering and viscos deformation of the ice matrix. We focused on the differences in the damage process depending on the loading rate to which the snow is subjected. Whereas for fast loading rates features indicating imminent failure are present in the AE, experimental results as well as simulations suggest that due to the rapid sintering and viscous deformation of the ice matrix the failure of snow seems difficult to be predicted for low loading rates. Hence applying AE techniques for snow avalanche prediction in the field seems not feasible. Still, the found AE characteristics may be useful to assess the mechanisms beyond the failure nucleation process that lead to the release of natural slab avalanches.

KEYWORDS: snow failure, avalanche release, precursor, acoustic emission, fiber bundle model

1. INTRODUCTION

In heterogeneous materials such as fiber composites, rocks, concrete, and snow, failure may occur as the culmination of a progressive damage process. In other words, failure does not occur by a "one-crack" mechanism, but instead by the complex interactions between multiple defects and micro-cracks (Sornette, 2006, p. 313). During the damage process acoustic emissions (AE) are generated, possibly due to micro-cracking. Those AE can be used to study how failure develops (e.g. Grosse and Ohtsu, 2008) and in some cases to predict failure (e.g. Amitrano et al., 2005; Faillettaz et al., 2011). For snow, the damage process and type failure strongly depend on the applied load or strain rate, whereas for fast loading rates snow fails in a brittle manner and for slow loading rates failure behavior is more ductile (Narita, 1980). This characteristic of snow is attributed to the peculiar mechanical properties of ice and the high homologous temperature under natural conditions, i.e. sintering or the formation of bonds between ice particle on contact and the creep or viscous deformation of the ice matrix.

* *Corresponding author address:*
Achille Capelli, WSL Institute for Snow and Avalanche Research SLF, Flüelastrasse 11, 7260 Davos Dorf, Switzerland;
tel: +41 81 417 02 52;
email: capelli@slf.ch

Recently, Capelli et al. (2018b) presented results of snow loading experiments with concurrent measurements of the AE preceding failure. They found not only the failure behavior (brittle vs. ductile) but also the AE response to depend on the loading rate. For correct interpretation of the observed AE features a model is needed that links the micromechanical mechanisms governing the damage process to the recorded AE.

Snow failure can be described with statistical fracture models such as the fiber bundle model (FBM) (e.g. Kun et al., 2006). The FBM consists of a high number of single elements (fibers) with heterogeneous strength, which obey simple mechanical (e.g. elastic deformation) and interaction (e.g. global vs. local load sharing) rules. From the interaction of the high number of single elements, the complex damage process of the bulk material is reproduced. A first attempt to model snow failure with a FBM was presented by Reiweger et al. (2009) to model displacement-controlled shear experiments. They reproduced the ductile-to-brittle transition in snow. More recently, a new version of a FBM including two healing mechanisms, sintering and load relaxation, was suggested for modeling the mechanical behavior of snow (Capelli et al., 2018a). This model presents effects similar to the observed dependence of the AE signatures during snow failure experiments.

Our aim is therefore to use the AE for studying the damage process prior to failure of snow, with

a particular focus on the occurrence of precursors and on the influence of the rate of loading on the AE response. Moreover, we aim to use a FBM for modeling the experiments and reproducing the experimentally observed AE signatures. We are particularly interested whether the FBM allows explaining the observed loading rate dependence of the AE signatures.

2. METHODS

2.1 Snow failure experiments

For the load-controlled snow failure experiments we used quadratic snow samples with a side length of 50 cm and a height of about 10 cm. The layered snow samples included in the middle a weak layer consisting of depth hoar crystals. For the snow failure experiments the snow samples were clamped between two metal plates and the load was increased linearly until the sample failed or the maximum load of 20 kPa was reached. We applied three different loading rates (32, 168, and 400 Pa s^{-1}) with an angle of 35° mimicking a typical avalanche slope angle. The applied load resulted in a progressive deformation of the samples, which was concentrated in the weak layer. At failure, a crack formed along the weak layer, and the weak layer eventually collapsed. During the loading process the generated AE were recorded by six wideband piezoelectric acoustic sensors (Mistras WD, 20-1000 kHz). This monitoring of AE allowed observing the ongoing damage process preceding failure. A more detailed description can be found in Capelli et al. (2018b).

2.2 Fiber bundle model

The FBM consists of a set of N fibers subjected to a load σ increasing with load rate $\dot{\sigma}$. The fibers have heterogeneous strength σ_{th} (Weibull distribution) mimicking the heterogeneity of snow. The load on the fibers is increased stepwise to the strength of the weakest fiber causing loading steps of variable duration $t = \frac{\Delta\sigma}{\dot{\sigma}}$. When the load on a fiber reaches its strength, the fiber fails and the load is redistributed among the surviving fibers (democratic or equal load sharing). The load redistribution may cause failure of other fibers and possibly initiating a cascade or burst of fiber ruptures. We added the following two features to this classical form of FBM.

(a) In analogy to the sintering mechanism of ice, each time the load increases the fibers can heal (sinter) and regain full strength, which is independent from the previous value. The load is zero immediately after sintering and increases with the external load or with load redistribution. We assume that the probability of forming a new bond depends on the amount of damage and increases with time. Therefore, the probability $p_{\mathrm{s},i}$ that a given broken fiber i re-sinters during the time interval Δt is:

$$p_{\mathrm{s},i}(\Delta t) = \left(1 - e^{-\frac{\Delta t}{t_{\mathrm{p}}}}\right)\frac{N_{\mathrm{broken}}}{N}, \quad (1)$$

and depends on the number of broken fibers N_{broken} as well as the characteristic sintering time t_{p} that controls the speed of the sintering process.

(b) We assume that the fibers are viscoelastic and each fiber can be described by a spring with elastic modulus E and a dashpot with viscosity η connected in series (Maxwell element). This viscoelasticity leads to time dependent relaxation of the load inhomogeneities that arise since the re-sintered fibers do not carry load initially. More specifically, the viscous deformation leads to an exponential relaxation of the single fiber load σ_i to the mean fiber load $\langle\sigma\rangle$ with:

$$\sigma_i(t + \ \ t) = \langle\sigma\rangle + (\sigma_i(t) - \langle\sigma\rangle)e^{-\frac{\Delta t}{t_{\mathrm{r}}}}, \quad (2)$$

with the characteristic relaxation time $t_{\mathrm{r}} = \frac{\eta}{E}$ controlling the relaxation speed.

The deformation of the fiber bundle is a superposition of elastic and viscous deformation. The detailed description of the model can be found in Capelli et al. (2018a).

3. RESULTS AND DISCUSSION

We exemplarily compare the FBM model results with the result of failure experiments at three loading rates (400, 168 and 32 Pa s^{-1}). The model parameters were calibrated by comparing the FBM to the experimental stress-strain relations (see Figure 1). Table 1 shows a list of the model parameters with the values we used in the comparison to the experiments. We adjusted the mean strength of the fibers $\langle\sigma_{\mathrm{th}}\rangle$ to fit the strength of the fiber bundle to the strength of the snow sample. The strength of the fibers follows a Weibull distribution with the shape factor k controlling the amount of disorder. The strength distribution should reflect the strength distribution of the elements of the ice matrix (bonds). Since no direct measurement method is available, we have to assume the type of distribution and the value of k. The speed of the sintering process is controlled by the sintering time t_{p}. For snow the characteristic time t_{p} is assumed to be constant (and therefore also the sintering speed). However, the relationship between sintering and damage speed changes when the loading rate changes. For the comparison with the snow experiments the parameter t_{p} was

adapted to meet the loading rate for which a transition in the failure behavior of snow was observed (between 32 and 168 Pa s^{-1}). Increasing the relaxation speed $t_r = \frac{\eta}{E}$ leads to faster load transfer from older fibers to younger fibers, which initially carry less load. Besides controlling the relaxation speed, the ratio of viscosity and elastic modulus also influences the bundle strain and its dependence on the loading rate. Therefore, viscosity and elastic modulus need to be adapted to the measured strain and the observed failure behavior. We determined the elastic modulus and the viscosity fitting the stress-strain relation of the model to the measured curves for the lowest and fastest loading rate (see Figure 1). The values of E and η are in good agreement with literature values for snow (Gerling et al., 2017; Mellor, 1975).

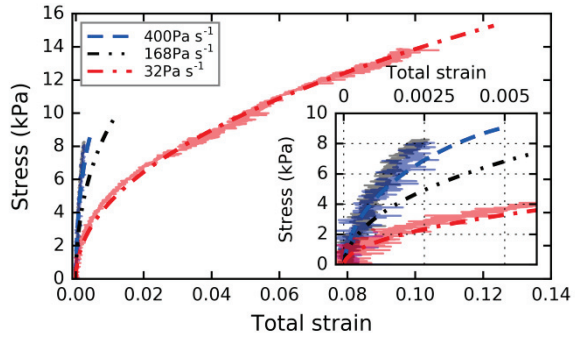

Figure 1: Stress-strain relations for both experiments (solid lines) and model (dash-dotted lines) and for three different loading rates. The inset shows a magnification of the strain range between 0 and 0.005.

Table 1: Model parameters and their values used for comparison to the experiments results.

Symbol	Description	Value	Units
N	Number of fibers	2.5×10^5	-
$\langle\sigma_{th}\rangle$	Mean strength of fibers	22.3	kPa
k	Shape factor of Weibull distr.	1.1	-
t_p	Characteristic sintering time	20	s
$t_r = \frac{\eta}{E}$	Characteristic relaxation time	2	s
E	Elastic modulus of snow	19	MPa
η	Viscosity	38	MPa s
$\dot{\sigma}$	Loading rate	32-400	Pa s^{-1}

The strain-stress relations of model and experiments are compared in Figure 1. At high loading rates (400 and 170 Pa s^{-1}), we observed low strain and brittle fracture of the snow samples. At low loading rate the strain at equal stress was much higher and the sample strength was higher. The FBM reproduced the higher strength and the higher strain at equal stress for lower loading rates. However, at low loading rates the model showed a divergence of the strain rate, which was not observed in the experiments. The strain rate divergence is caused by a divergence of the number of intact fibers carrying load and the resulting increase of the load per fiber.

The recorded acoustic energy E_{AE} is an indication of the amount of damage generated in the snow sample. Using the amount of energy per unit stress instead of energy per time allows comparing the increase of damage with increasing stress for the different loading rates. Hence, the remainder of the text, we refer to the energy rate as the energy rate of change with stress $\frac{dE_{AE}}{d\sigma}$. We assume that when the fibers fail, this elastic energy is dissipated partially as AE, and that the AE energy E_{AE} produced by the microscopic damage is proportional to the elastic energy U stored in the breaking fibers. Therefore, we can compare the model elastic energy rate $\frac{dU}{d\sigma}$ with the experimental energy rate $\frac{dE_{AE}}{d\sigma}$ (Figure 2).

For the experiment, we observed an exponential increase of the energy rate toward failure and the exponential coefficient (slope in Figure 2a) was higher for the higher loading rate. The model showed a similar behavior, with an approximately exponential increase of the energy rate with increasing load (if the vicinity of the failure is disregarded) and higher exponential coefficient for higher loading rate. However, for the high loading rates the model showed a divergence of the energy rate close to failure, which has the same cause as the divergence of the strain rate.

The probability density functions of the AE events energy E_{AE}, and of the modeled burst elastic energy U were power-law distributed. The power-law distribution is characterized by the exponent, which is usually referred to as the b-value. Of particular interest is the evolution of the b-value with increasing load (Figure 3), since it indicates variations of the event statistics towards failure and is considered a useful precursor for failure prediction (Amitrano, 2012; Amitrano et al., 2005; Capelli et al., 2018b).

For the snow failure experiments a decrease of the b-value with increasing load was observed for the higher loading rates, whereas for the slower loading rates the b-value was constant. Moreover, the b-value at failure was higher for lower loading rates.

For the FBM similar results were obtained for the b-value of the energy U (Figure 3b). The FBM with sintering and load relaxation reproduced the higher b-value at failure for lower rates observed for the experiments. However, the b-value de-

creased for all loading rates. According to the theory of critical phenomena the observed AE features for the high loading rates can be interpreted as a transition from a stable state with uncorrelated damage to an unstable state with correlated damage leading to complete failure. At low loading rates (32 Pa s^{-1}) the AE features indicated a stable state of the damage process over the entire duration of the experiment, and we assume that during slow loading the damage process was balanced by the healing process.

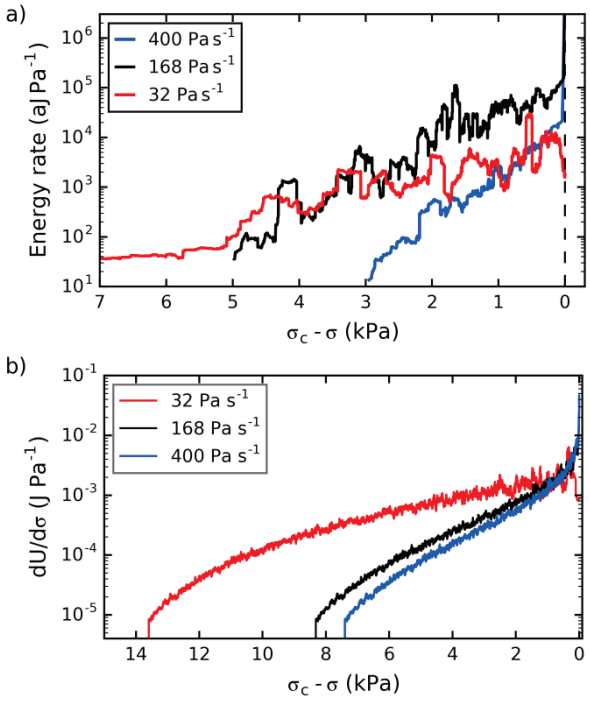

Figure 2: (a) Evolution of AE energy rate $\frac{dE_{AE}}{d\sigma}$ toward failure for three snow failure experiments with different loading rates. (b) Evolution FBM elastic energy rate $\frac{dU}{d\sigma}$ (emitted energy per unit stress) with increasing load.

The good agreement of modeled and experimental results is remarkable considering the simplicity of the model and it confirms that the FBM is a valuable tool for studying the effects of basic microscopic mechanisms on the macroscopic failure behavior.

Moreover, we showed that adding viscous deformation and the resulting load relaxation, the FBM exhibited features that cannot be reproduced with models incorporating only sintering (Capelli et al., 2018b).

However, many current models used for studying snow failure do not consider any healing mechanism (Gaume et al., 2015) or consider only sintering (e.g. Gaume et al., 2017; Reiweger et al., 2009; Steinkogler et al., 2015). Our results show the necessity of considering both time dependent mechanisms (sintering and load relaxation) for modeling snow failure for low loading rate or for modeling natural snow avalanches where slow loading rates are involved.

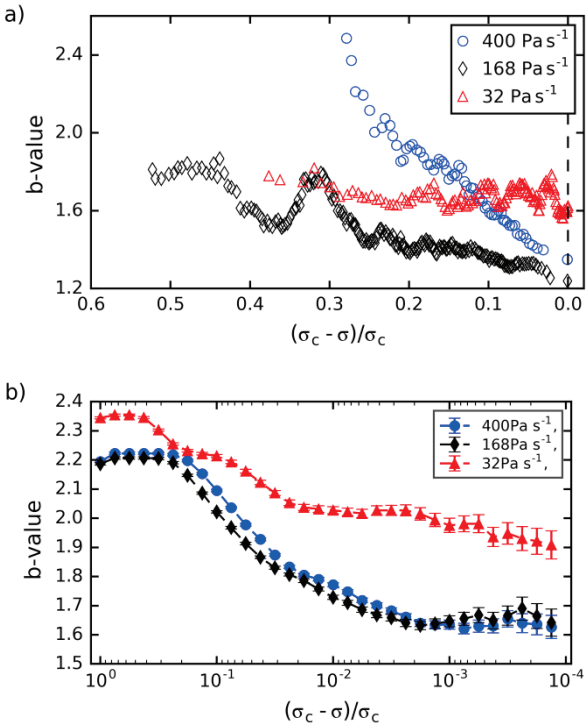

Figure 3: Evolution of b-value with increasing load σ up to failure at σ_c for three different loading rates for: (a) AE energy E_{AE} for the snow failure experiments, and (b) for the FBM burst elastic energy U.

For high loading rates the AE showed some features that could be used to predict failure or identify unstable states of the snow. The exponential increase of the energy rate and mainly the decrease of the b-value indicate imminent failure. The divergence of the energy rate at failure present for the model can be used to determine the point of failure, but was not present in the AE signals of the experiments.

On the other hand, for low rates both experiments and model indicated that the failure occurs abruptly without any of the typical precursors. The b-value of the AE was constant over the entire experiment and the energy rate increase was more moderate. Also for the model the b-value decreased to a higher value at failure.

The lack of clear precursors that indicate imminent failure for both low and high loading rates makes the application of AE for avalanche prediction questionable. In particular considering that the load increase due to precipitation, which is believed to cause the nucleation of the initial crack is quite slow. However, the observed difference in the AE signature in dependence of

the loading rate may be used to investigate which of the two types of damage process is involved in the formation of natural avalanches. This feature may help to better understand as well as better model how the initial failures form that lead to avalanche release.

4. CONCLUSIONS

We performed snow failure experiments at different loading rates and concurrently measured the acoustic emissions to study the influence of the loading rate on the progressive damage process prior to failure. Moreover, we modeled the snow failure experiments with a fiber bundle model (FBM) including two healing mechanisms: (a) sintering which corresponds to regenerating broken fibers with time dependent probability, and (b) viscous deformation of the fibers resulting in time dependent relaxation of load inhomogeneities. The FBM allowed reproducing the loading rate dependent stress-strain relations observed in the snow failure experiments. Moreover, the FBM exhibited AE features similar to the observed loading rate dependent AE features occurring before snow failure.

Our results indicate that both sintering and viscous deformation with resulting load relaxation are essential for modeling snow failure. These processes are of particular relevance when modeling natural release of snow avalanches where slow loading conditions are involved. Whereas for high loading rate some features that may indicate imminent failure were identified, for low loading rates the failure occurred suddenly without precursors for both experiment and model. Therefore, applying AE techniques for avalanche prediction seem not to be feasible, at least for the time being with the methods we used.

ACKNOWLEDGEMENTS

This project was funded by the Swiss National Science Foundation (SNF), project number 200021-146647.

REFERENCES

Amitrano, D., 2012. Variability in the power-law distributions of rupture events - How and why does b-value change. Eur. Phys. J.-Spec. Top., 205(1): 199-215.

Amitrano, D., Grasso, J.R. and Senfaute, G., 2005. Seismic precursory patterns before a cliff collapse and critical point phenomena. Geophys. Res. Lett., 32(8): L08314.

Capelli, A., Reiweger, I., Lehmann, P. and Schweizer, J., 2018a. Fiber bundle model with time-dependent healing mechanisms to simulate progressive failure of snow. Phys. Rev. E: in press.

Capelli, A., Reiweger, I. and Schweizer, J., 2018b. Acoustic emissions signatures prior to snow failure. J. Glaciol., 64(246): 543-554.

Faillettaz, J., Funk, M. and Sornette, D., 2011. Icequakes coupled with surface displacements for predicting glacier break-off. J. Glaciol., 57(203): 453-460.

Gaume, J., Löwe, H., Tan, S. and Tsang, L., 2017. Scaling laws for the mechanics of loose and cohesive granular materials based on Baxter's sticky hard spheres. Phys. Rev. E, 96(3): 032914.

Gaume, J., van Herwijnen, A., Chambon, G., Birkeland, K.W. and Schweizer, J., 2015. Modeling of crack propagation in weak snowpack layers using the discrete element method. Cryosphere, 9: 1915-1932.

Gerling, B., Löwe, H. and van Herwijnen, A., 2017. Measuring the elastic modulus of snow. Geophys. Res. Lett., 44(21): 11088-11096.

Grosse, C.U. and Ohtsu, M., 2008. Acoustic emission testing. Springer, Berlin Heidelberg, Germany, 406 pp.

Kun, F., Hidalgo, R.C., Raischel, F. and Herrmann, H.J., 2006. Extension of fibre bundle models for creep rupture and interface failure. Int. J. Fracture, 140(1-4): 255-265.

Mellor, M., 1975. A review of basic snow mechanics, Symposium at Grindelwald 1974 - Snow Mechanics, IAHS Publ., 114. International Association of Hydrological Sciences, Wallingford, Oxfordshire, U.K., pp. 251-291.

Narita, H., 1980. Mechanical behaviour and structure of snow under uniaxial tensile stress. J. Glaciol., 26(94): 275-282.

Reiweger, I., Schweizer, J., Dual, J. and Herrmann, H.J., 2009. Modelling snow failure with a fiber bundle model. J. Glaciol., 55(194): 997-1002.

Sornette, D., 2006. Critical Phenomena in Natural Sciences. Springer Series in Synergetics. Springer-Verlag, Berlin, Germany, 528 pp.

Steinkogler, W., Gaume, J., Löwe, H., Sovilla, B. and Lehning, M., 2015. Granulation of snow: From tumbler experiments to discrete element simulations. J. Geophys. Res.-Earth Surf., 120(6): 1107-1126.